Fault Diagnostics and Prognostics for Large Segmented SRMs

Dmitry G. Luchinsky[1,2] and Viatcheslav V. Osipov[1,2], Vadim N. Smelyanskiy[2], Dogan A. Timucin[2], Serdar Uckun[2]
[1]Mission Critical Technologies Inc., 2041Rosecrans Ave. Suite 225 El Segundo, CA 90245
[2]NASA Ames Research Center, Mail Stop 269-2, Moffett Field, CA 94035, USA, Vadim.N.Smelyanskiy@nasa.gov,

Ben Hayashida, Michael Watson
NASA Marshall Space Flight Center, Huntsville, Alabama 35812

Joshua McMillin, David Shook, Mont Johnson, Scott Hyde
ATK Thiokol, Large Salt Lake City Area, Utah

Abstract—We report progress in development of the fault diagnostic and prognostic (FD&P) system for large segmented solid rocket motors (SRMs). The model includes the following main components: (i) 1D dynamical model of internal ballistics of SRMs; (ii) surface regression model for the propellant taking into account erosive burning; (iii) model of the propellant geometry; (iv) model of the nozzle ablation; (v) model of a hole burning through in the SRM steel case. The model is verified by comparison of the spatially resolved time traces of the flow parameters obtained in simulations with the results of the simulations obtained using high-fidelity 2D FLUENT model (developed by the third party). To develop FD&P system of a case breach fault for a large segmented rocket we notice [1] that the stationary zero-dimensional approximation for the nozzle stagnation pressure is surprisingly accurate even when stagnation pressure varies significantly in time during burning tail-off. This was also found to be true for the case breach fault [2]. These results allow us to use the FD&P developed in our earlier research [3]-[6] by substituting head stagnation pressure with nozzle stagnation pressure. The axial corrections to the value of the side thrust due to the mass addition are taken into account by solving a system of ODEs in spatial dimension.[1]

TABLE OF CONTENTS

NOMENCLATURE

ρ = gas density
p = gas pressure
T = gas temperature
u = gas velocity
e = internal energy of the combustion gases
c_V = specific heat for constant volume
c_p = specific heat for the constant pressure
l = perimeter of propellant cross-section
R = burn distance of the propellant
λ = coefficient of surface friction
A_p = port area
A_t = cross-sectional area of the nozzle throat
A_b = total area of the burning surface
v_m = velocity of metal melting front
v_n = velocity of nozzle ablation front
c = sound velocity
M = Mach number, $M = u/c$
γ = ration of specific heats $\gamma = c_P/c_V$
r_b = burning rate of solid propellant
r_c = reference burning rate
n = exponent for burning rate of the propellant
p_c = reference pressure for burning rate
p_{ns} = nozzle stagnation pressure
a = constant for burning rate [$a = r_c/p_c^n$]
r_{er} = rate of erosive burning of solid propellant
ρ_p = density of the solid propellant
Re = Reynolds number
e_t = total energy of the gas
h_t = total enthalpy of the gas
R_n = radius of nozzle throat
R_h = radius of the hole
r_{met} = radius of hole in metal case
L = length of the propellant grain
F_N = normal thrust
F_h = additional thrust produced by hole gas flow
n = exponent for burning rate of the propellant
h_p = combustion heat of the solid propellant
Q = heat flow from the gas to the walls of the hole
Q_c = convection heat flow
Q_R = radiation heat flow
Q_c = heat flow from burning metal to its surface
T_{mel} = melting temperature point
T_{m0} = temperature of metal far from hole
T_{ms} = temperature of metal surface in the hole throat
T_{abl} = critical temperature of the nozzle ablation
T_c = temperature of metal case far from hole
C_m = specific heat of case metal
q_m = latent heat of metal melting
ρ_m = density of case metal
k = the thermal conductivity

1

[1] 978-1-4244-2622-5/09/$25.00 ©2009 IEEE.
[1] IEEEAC paper #1001, Version 5, Updated May 31, 2008

v_{fb} = velocity of the metal burning front
μ = dynamical viscosity of hot gas
Pr = the Prandtl number, Pr=$\mu C_p/k$
σ = Stefan-Boltzmann constant
Subscripts:
h = for gas parameters in the hole
ht = for the gas parameters in the hole throat
N = for parameters in normal regime
0 = for stagnation values of gas parameters
N_t = nozzle throat
N_{ex} = nozzle exit
m = for metal parameters
abl = ablation

1. INTRODUCTION

Safety of the manned space missions requires development of a novel IVHM system for solid rocket motors. In our earlier work [3]-[6] we have introduced a model based fault diagnostic and prognostic system for a subscale SRM. It was shown that the system can incorporate the following characteristic features of the SRMs ballistics: (i) highly nonlinear SRM internal hydrodynamics, (ii) identify a number of failure modes, (iii) severely limited number and types of sensors available onboard, and (iv) small recovery time. The performance of our FD&P system was verified using 2D high-fidelity FLUENT modeling and the results of the ground firing test. Some results obtained for the subscale motor can be extended to a case breach model of large SRMs. In particular, the LDPM of the nozzle stagnation pressure, nozzle ablation model, and hole growth model can be adapted to the SRM. However, the extension of this system to large segmented rockets is complicated due to the following reasons. Firstly, the effect of the mass addition [1],[7] has to be taken into account to calculate the pressure distribution along the axis of the large rocket. Secondly, realistic modeling of the fault-induced side thrust requires calculations of a complex pattern of the shock waves developed in a free supersonic flow at the outlet of the hole of the case breach. An additional difficulty in modeling internal ballistics of the large segmented SRMs is related to the fact that the propellant burning model has to be extended by including the corrections for erosive burning and friction.

In this paper we describe a 1-D dynamical model of the internal ballistics of a multi-segment SRMs. Our model describes the nominal regime as well as the off-nominal regime in the presence of a case breach fault. The developed model of the case breach allows calculations of the side thrust at a given location along the rocket axis. The model takes into account the effect of mass addition along the rocket axis, erosive burning, and surface friction. Two algorithms: the algorithm for integration of this model in quasi-steady approximations and FD&P algorithm for reconstructing and predicting case breach fault dynamics in real time from the measurements of the head pressure are introduced. The results of the calculations of the internal ballistics in nominal regime are verified by comparison with the results of the simulations obtained using high-fidelity 2D FLUENT model (developed by third party). The results of the calculations in the off-nominal regime are verified by comparison with the earlier results of the 1st Stage Malfunction Turn Study of the case breach failure [2].

2. MODEL

To model internal ballistics of the SRM we use the system of equations for the mass, momentum and energy conservation in one-dimension

$$\partial_t\left(UA_p\right)+\partial_x\left(f(U)A_p\right)=S \tag{1}$$

$$U=\begin{bmatrix}\rho\\ \rho u\\ \rho e_T\end{bmatrix},\quad f(U)=\begin{bmatrix}\rho u\\ \rho u^2+p\\ \rho u e_T+up\end{bmatrix},$$
$$S=\begin{bmatrix}\rho_p\dot{R}l(x)+a_1\xi_1(t)\\ p\partial_x A_p-\lambda\rho u^2 l(x)+a_2\xi_2(t)\\ h_p\rho_p\dot{R}l(x)+a_3\xi_3(t)\end{bmatrix} \tag{2}$$

Here x is the coordinate along the motor axis, $e_T = e + u^2/2$, $h_T = e_T + p/\rho = h + u^2/2$, $h = c_pT$, $e = c_vT$, $\xi_i(t)$ are white zero-mean Gaussian noises with amplitudes a_i. It is assumed that everywhere in the combustion chamber and in the nozzle the following equation of state for an ideal gas holds

$$\frac{p}{\rho}=(c_P-c_V)T=\frac{p_0}{\rho_0}\left(\frac{T}{T_0}\right)=\frac{c_0^2}{\gamma}\left(\frac{T}{T_0}\right) \tag{3}$$

The burning rate taking into account the erosive burning is

$$\dot{R}=r_b=ap^n+r_{er}\ . \tag{4}$$

The erosive correlation is of the form

$$r_{er}=C\left(I-I_{cr}\right), \tag{5}$$

for $I > I_{cr}$ and zero otherwise, where C and I_{cr} are constants. Here $I=const\left(\rho u\ /\ r_b\rho_p\right)\mathrm{Re}^{-1/8}$.

To model the actual propellant geometry the combustion chamber is divided into N segments along the rocket axis as schematically shown in the Figure 1. For each segment "i" the port area $A_p(x_i)$ and perimeter $l(x_i)$ averaged over the segment length dx_i are provided in the form of the design curves (DCs) (see the Figure 1)

$$A_p(x_i)=f_{Ai}(R(x_i)),\ l(x_i)=f_{Ai}(R(x_i)). \tag{6}$$

Note that the port volume and burning area for each segment are given by the following relations

$$dV(x_i)=A_p(x_i)dx_i,\ \ dA_b(x_i)=l(x_i)dx_i. \tag{7}$$

The model of the nozzle ablation is taken in the form corresponding to the Bartz' approximation [8]-[10] as

$$\dot{R}_N=v_{t0}\left(\frac{\rho u}{(\rho u)_{\max}}\right)^{1-\beta}\left(\frac{R_N}{R_{N0}}\right)^{-\beta}\frac{\left(T-T_{abl}\right)}{\left(T_t-T_{abl}\right)}.$$

In a particular case of the ablation of the nozzle throat and nozzle exit this approximation takes the form

$$\dot{R}_{Nt} = \tilde{v}_{t0}\left(\frac{p_0}{p_{\max}}\right)^{1-\beta}\left(\frac{R_{Nt}}{R_{Nt0}}\right)^{-\beta} \quad (8)$$

$$\dot{R}_{Nex} = v_{e0}\left(\frac{p_0 S_{Nt}}{p_{\max} S_{Nex}}\right)^{1-\beta}\left(\frac{R_{Nex}}{R_{Nex0}}\right)^{-\beta}\frac{(T-T_{abl})}{(T_t-T_{abl})} \quad (9)$$

where $R_{Nt0} = R_{Nt}(0)$, $R_{Nex0} = R_{Nex}(0)$ and

$$\tilde{v}_{t0} = C\left(\frac{\gamma p_{\max}}{\Gamma c_0}\right)^{1-\beta}\left(\frac{2R_{Nt0}}{\mu}\right)^{-\beta}\frac{(T_* - T_{abl})}{[c_{in}(T_{abl}-T_0)+q_{in}]} \quad (10)$$

To complete the model of the case breach fault for the segmented SRM the system of equations (8)-(9) above has to be extended by including equations of the hole growth model [4]-[6]

$$\dot{R}_h = v_h(p_{th}, T_t) = \frac{Q_c + Q_R + Q_b}{\left[q_m + C_m\left(T_{mel} - T_{m0}\right)\right]\rho_m}, \quad (11)$$

$$Q_R = \sigma\left[1-\exp\left(-\lambda p_{ht}\right)\right]\left(T_{ht}^4 - T_{ms}^4\right),$$

$$Q_c = 0.023 c_p\left(\frac{\gamma p_{ht}}{\Gamma c_0}\right)^{0.8}\left(\frac{2R_{ht}}{\mu}\right)^{-0.2}\left(T_t - T_{ms}\right), \quad (12)$$

$$Q_b = v_{fb}\left[q_m + C_m\left(T_{mel} - T_{m0}\right)\right]\rho_m.$$

The main rocket thrust and lateral (side) thrust F_h induced by the gas flow through the hole are given in the form

$$F_N = J_t c_0 M_{ex}\varphi_G + (p_{ex} - p_{atm})A_{ex}, \quad (13)$$

$$F_h = J_h c_0\left(\frac{2}{\gamma+1}\right)^{1/2} + (p_{ht} - p_{atm})A_{ht}. \quad (14)$$

where $J_t = \rho_t u_t A_t$ and $J_h = \rho_{ht} u_{ht} A_{ht}$ are mass flows through the nozzle throat and hole throat.

The model of the case breach fault for the large segmented RSRM can be briefly summarized as follows

$$\begin{cases} \partial_t\left(UA_p\right) + \partial_x\left(f(U)A_p\right) = S, \\ A_p(x_i) = f_{Ai}(R(x_i)), \qquad l(x_i) = f_{li}(R(x_i)), \\ \dot{R} = ap^n + C\left(I - I_{cr}\right), \\ \dot{R}_{Nt} = v_{t0}\left(\frac{p_0}{p_{\max}}\right)^{1-\beta}\left(\frac{R_{Nt}}{R_{Nt0}}\right)^{-\beta}, \\ \dot{R}_{Nex} = v_{e0}\left(\frac{p_0 S_{Nt}}{p_{\max} S_{Nex}}\right)^{1-\beta}\left(\frac{R_{Nex}}{R_{Nex0}}\right)^{-\beta}\frac{(T-T_{abl})}{(T_t-T_{abl})}, \\ \dot{R}_h = \frac{Q_c + Q_R + Q_b}{\left[q_m + C_m\left(T_{mel} - T_{m0}\right)\right]\rho_m}, \end{cases} \quad (15)$$

with definitions of the parameters given in the equations above. The difference between the model (15) and the sub-scale model introduced in our earlier research [3]-[6] is that: (i) gas dynamics in (15) is governed by a set of PDEs (cf [1],[7],[11]) instead of set of ordinary differential equations (ODE) as before, (ii) the burning law takes account of erosive burning, and (iii) and the geometry of the rocket is given by a set of N design curves for port area and port perimeter in N locations instead of one design curve for total burning area as a function of the burn distance as before.

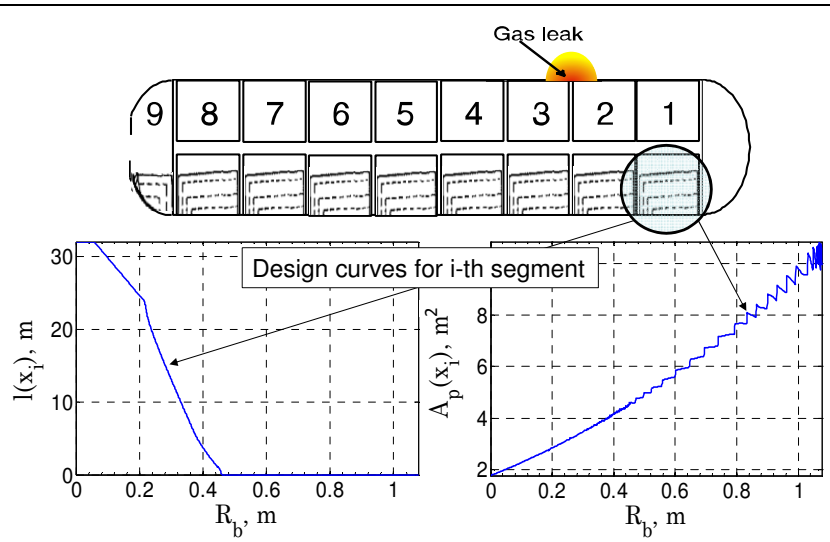

Figure 1 Sketch of a cross-section of an idealized geometry of the multi-segment SRM rocket and an example of the design curves (6) for the head section of the SRM

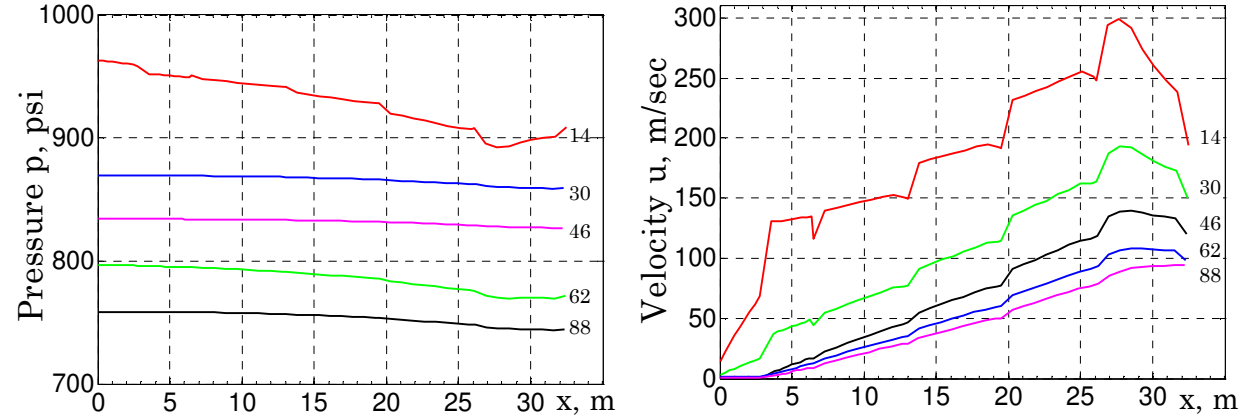

Figure 2. Solution of the BVP (17), (18) for pressure (left) and velocity (right) axial distributions at different moments of time. Time after ignition: (14, 30, 46, 62, 88) seconds. *x* is measured from the motor head.

Accordingly both the numerical integration of this model and diagnostics and prognostics of the fault dynamics are different as will be described below.

3. NUMERICAL SOLUTION

To integrate system (15) we notice that (15) is a system of nearly balanced PDEs with slowly varying parameters. This is an example of PDEs with multiple time scales [12], where the slower dynamical time scale is a result of a near balance between $\partial_x(f(U)A_p)$ and S in the first eq. in (15) and from slowly varying parameters described by the last four eqs. in (15). The fast dynamics of (15) corresponds to the acoustic time scale. To see the multiple time scale character of the system (15) more clearly let us introduce dimensionless variables

$$p \to \frac{p}{p_0}, \rho \to \frac{\rho}{\rho_0}, \rho_p \to \frac{\rho_p}{\rho_0}, T \to \frac{T}{T_0}, R_N \to \frac{R_N}{L_0}, \quad (16)$$
$$t \to \frac{t}{t_0}, R \to \frac{R}{L_0}, l \to \frac{l}{L_0}, A_p \to \frac{A_p}{L_0^2}, u \to \frac{u}{c_0} = M_0;$$

where $t_0 = L_0/ap_0^n \approx 10^{-2}$ sec and $L_0 \approx 1$m are characteristics scales of time and length. In dimensionless variables the PDEs can be rewritten as follows

$$\partial_x A_p \begin{bmatrix} \rho M_0 \\ \gamma\rho M_0^2 + p \\ \rho M_0\left(T + \frac{\gamma-1}{2}M_0^2\right) \end{bmatrix} = \begin{bmatrix} \delta\rho_p \dot{R} l(x) \\ p\partial_x A_p - \gamma\lambda\rho M_0^2 l(x) \\ \delta\rho_p \dot{R} l(x) \end{bmatrix} \quad (17)$$
$$-\delta\partial_t A_p \begin{bmatrix} \rho \\ \rho M_0 \\ \rho\left(T/\gamma + \frac{\gamma-1}{2}M_0^2\right) \end{bmatrix}$$

Here we have introduced small parameter $\delta = L_0/(t_0 c_0) = (ap_0^n)/c_0 \approx 10^{-5}$ corresponding to the ratio of the characteristic velocity of the propellant surface regression ($ap_0^n \approx 10^{-2}$m/sec) to the speed of sound ($c_0 \approx 1006$m/sec). It is clear that in the first approximation at each given moment of time the axial distribution of the flow variables in a segmented rocket can be found in quasi-steady approximation neglecting a small last term proportional to $\delta \approx 10^{-5}$. Note that two source terms in the 1st and 3rd eqs. of (17) are also $\propto\delta$ but these terms cannot be neglected, because they are prop to $\rho_p \approx 10^2$.

To solve equations (17) one can neglect the last term $\propto \delta$ and complete the resulting system of ODEs by a set of boundary conditions. The boundary conditions at the aft end (at the outlet of the grain) are defined by the choking (sonic) conditions at the nozzle throat. The boundary conditions at the rocket head are determined by the continuity conditions of the gas flow from the propellant surface and through the port area at the rocket head. By adding to these two conditions the equation of state and the equation for the gas temperature in the combustion chamber as a function of the Mach number M_0 we obtain resulting boundary conditions at the rocket head (H) and aft (A) ends in dimensionless units as follows

$$M_{0,H} = \left(\frac{\delta\rho_p A_{b,H}}{A_{p,H}}\right)\left(1 - \frac{\gamma-1}{2}M_{0,H}^2\right)p_H^{n-1},$$
$$M_{0,A}\left(1 - \frac{\gamma-1}{2}M_{0,A}^2\right)^{\frac{1}{\gamma-1}} = \frac{A_t}{\Gamma A_A}, \quad (18)$$
$$p_A = \rho_A\left(1 - \frac{\gamma-1}{2}M_{0,A}^2\right).$$

Using (3) the set of equations for boundary conditions can be reduced to three independent equations. The resulting axial distributions of the pressure and velocity are shown in the **Figure 2** for five instances of time with the time step 16 sec (the time resolution of the solution was 0.2sec). It can be seen from the figure that there is a substantial difference between the head and aft pressure due to the effect of mass addition. The difference is most significant at the initial time when the port area is the smallest and the flow velocity has the largest values along the axis. With time the port area is increasing and the difference between head and aft pressure becomes negligible.

4. FAULT PREDICTION

More accurate predictions of the fault-induced internal

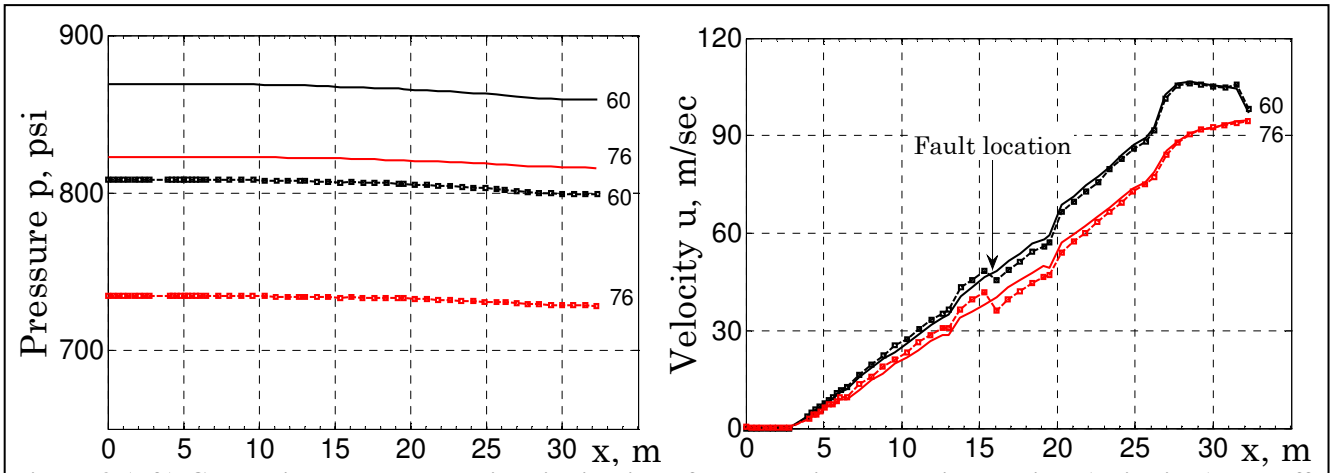

Figure 3 (left) Comparison between spatial distribution of pressure in the nominal regime (solid lines) and off-nominal regime (squares). (right). Comparison between spatial distribution of velocity in the nominal regime (solid lines) and off-nominal regime (circles). The time instants from the top to the bottom in the figure are 60 sec and 76 sec. The time resolution of the calculations was 0.2 sec, initial radius of the hole R_{h0} = 1 in, burning rate of the hole wall v_m = 0.3 in/sec, initial time of the fault 20 sec, the fault is located in the middle section.

ballistics of the segmented SRM that can be obtained by solving the BVP for the system (17), (18) require more accurate estimations of the fault-induced perturbations of the first three equations in system (18). In the presence of the fault at location x_h these equations can be rewritten as follows (in dimensionless variables)

$$\partial_x A_p \begin{bmatrix} \rho M_0 \\ \gamma p M_0^2 + p \\ \rho M_0 \left(T + \frac{\gamma-1}{2} M_0^2 \right) \end{bmatrix} = \begin{bmatrix} \delta \rho_p \dot{R} l(x) \\ p \partial_x A_p - \gamma \lambda \rho M_0^2 l(x) \\ \delta \rho_p \dot{R} l(x) \end{bmatrix} - \partial_x A_h \begin{bmatrix} \rho_t M_{0,t} \delta(x - x_h) \\ 0 \\ \rho_t M_{0,t} T_t \delta(x - x_h) \end{bmatrix} \tag{19}$$

With boundary conditions at the aft and head ends (18) and dimensionless flow variables at the hole throat location given by following expressions

$$M_{0,t}(x_h) = \left(\frac{\gamma+1}{2} \right)^{-1/2}, \quad T_t(x_h) = \left(\frac{\gamma+1}{2} \right)^{-1}$$
$$\rho_t(x_h) = \left(1 - \frac{\gamma-1}{2} M_0^2(x_h) \right)^{\frac{-1}{\gamma-1}} \left(\frac{\gamma+1}{2} \right)^{\frac{-1}{\gamma-1}}. \tag{20}$$

The results of the predictions of the spatial distributions of the segmented SRM in the presence of the fault located at the joint between central and central aft segments are shown in the **Figure 3.** It is important to notice that the case breach fault induces practically uniform shift of the pressure along the rocket axis. The differences in the shifts between the head and aft ends of the rocket remain very small. These features pave the way to the in-flight diagnostics and prognostics of the fault parameters using the head pressure as a reference (as will be explained in more details below) despite the fact that the mass addition is playing an important role in the pressure build up along the rocket axis of large segmented SRM.

5. FD&P FOR THE CASE BREACH FAULT

It was shown in the previous section that pressure changes induced by the case breach fault are uniform along the motor axes. We notice [1] that the stationary zero-dimensional approximation (21)

$$p_{ns}(t) = \left[\frac{\Gamma c_0 \rho_p a}{\gamma} \left(\frac{A_{b,eff}(t)}{A_t(t) + A_h(t)} \right) \right]^{\frac{1}{1-n}}. \tag{21}$$

for the nozzle stagnation pressure (p_{ns}) holds surprisingly accurate even when stagnation pressure varies significantly in time during burning tail-off. This was also found to be true for the case breach fault [2]. To further improve the accuracy of this approximation it was also suggested in our earlier research [3]-[6] to introduce an effective burning area $A_{b,eff}(t)$. These findings suggest that an FD&P algorithm for the case breach fault can be developed as an extension of the corresponding algorithm for a sub-scale motor developed in our earlier research [3]-[6]. The important change is that the pressure is measured at the head of the motor, while the eq. (21) is written for the nozzle stagnation pressure.

To take into account the change described above the following algorithm can be used:

1) Use nominal regime time-traces to determine the effective burning area by inverting eq. (21)

$$A_{b,eff}(t) = \left[\frac{\gamma A_t(t)}{\Gamma c_0 \rho_p a} \right] p_{ns}^{1-n}(t);$$

2) Use measured time-trace of the head pressure in the off-nominal regime $p_H(t)$ to find fault-induced pressure at the aft end using the fact that the pressure changes induced by the fault are uniform along the motor axis

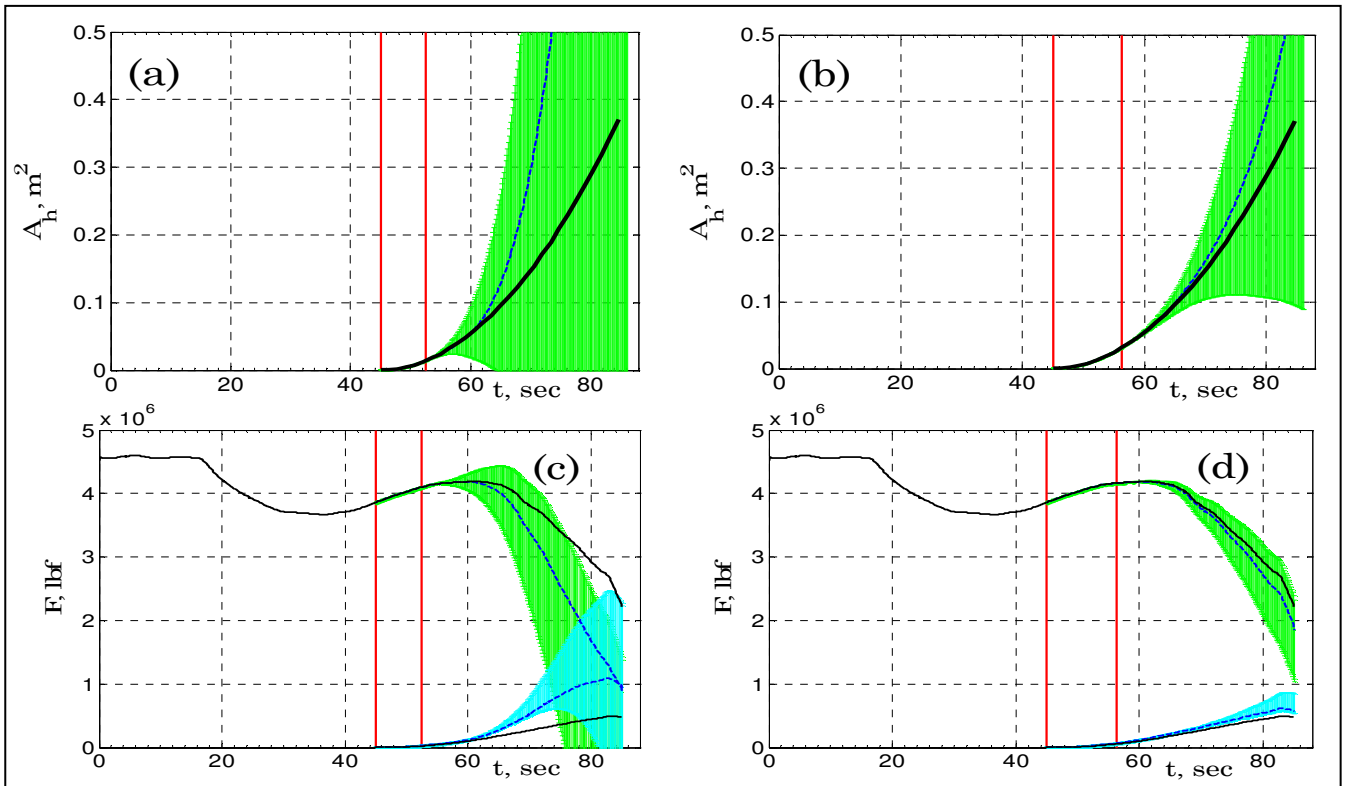

Figure 4 Convergence of the predicted hole area (top) and thrust (bottom). The actual time-traces (black solid lines) are compared with the time-traces of mean predicted values (blue dashed lines). The green shading indicates standard deviations for the predicted values of area, pressure and rocket thrust. The cyan shading indicates standard deviations for predicted value of the side thrust. In the figures the prediction is made after ΔT_m=8 sec (left) and ΔT_m=11 sec (right). The beginning and the end of the time interval used to infer fault parameters are indicated by red vertical lines. Fault initial time T_f = 45 sec in all cases, initial hole radius 0.35 in, metal burning rate 0.325 in/sec.

$$p_A^{(fault)}(t) = p_A^{(nom)}(t) + \left(p_H^{(fault)}(t) - p_H^{(nom)}(t) \right);$$

3) Use nominal time-trace of the Mach number at the aft end to determined nozzle stagnation pressure

$$p_{ns}^{(fault)}(t) = p_A^{(fault)}(t) \left(1 - \frac{\gamma - 1}{2} M_{A,0}^2(t) \right)^{-1};$$

4) Use inverted eq. (21) to determined time-trace of the hole area $A_h(t) = A_t(t) + \left[\frac{\Gamma c_0 \rho_p a A_{b,eff}(t)}{\gamma \left(p_{ns}^{(fault)}(t) \right)^{1-n}} \right]$.

Note that the most probable earliest time of occurrence of the case breach fault is at the end of the burning out time and therefore the algorithm above can be applied with high accuracy to the aft motor pressure. In what follows we will be using $p_A^{(fault)}(t)$ as a substitute for $p_{ns}^{(fault)}(t)$ without further comments.

We now verify this algorithm by numerical simulations in the presence of the noise in the time-traces of pressure. In this test the fault initial time T_f = 45 sec in all cases. The hole radius growth rate is ≈ 0.325 in/sec. The initial radius of the hole is ≈ 0.35in. The noise intensity of the pressure measurements was 0.02%. The time intervals ΔT_m used to infer fault parameters are 8 sec and 11 sec. The predictions are made up to 85 sec of the flight. The resulting predicted time-traces of the hole area, pressure, rocket and hole thrusts are shown in the Figure 4. It can be seen that convergence is achieved 11 sec after the fault initiation, when hole radius is ≈ 3.85in and pressure deviation from the nominal value is ≈ 2.5%. The higher levels of measurement noise will further degrade the accuracy of predictions.

CONCLUSIONS

1-D model of internal ballistics of a large segmented solid rocket motor is presented that takes into account: (i) exact geometry of the grain and the regression of the propellant surface as a given function of burning distance; (ii) erosive burning; (iii) surface friction; (iv) nozzle ablation; (v) breach of the rocket case. The model is integrated in quasi-steady approximation by solving the boundary value problem using shooting method. The results of integration were verified by comparison with 2D FLUENT simulations (developed by the third party). FD&P is introduced to reconstruct parameters of the case breach and predict its dynamics in real time from the measurements of head pressure time-traces. The algorithm converges 15 sec after fault initiation for the measurements noise 0.02%. The results of the predictions were verified by comparison with the results of 1st Stage Malfunction Turn Study of the case breach failure [2]. We conclude that it is possible at least in

principle to build FD&P system for the in-flight detection and prediction of the case breach. The accuracy of the algorithm is limited by the sampling rate and by the accuracy of the approximation of the effective burning area that relates the total burning area to nozzle stagnation pressure via relation (21). The method can be applied quite generally to the analysis of a number of other faults in SRMs.

REFERENCES

[1]. M. Salita, AIAA 89-0298, 27th Aerospace Sciences Meeting (Reno), 1/10/89.

[2]. J. E. McMillin, AIAA 2006-5121, 42nd AIAA/ ASME/SAE/ASEE Joint Propulsion Conference & Exhibit 9 - 12 July 2006, Sacramento, California.

[3]. V.V. Osipov, D.G. Luchinsky, V.N. Smelyanskiy, D.A. Timucin, AIAA-2007-5823, 43rd AIAA/ ASME/SAE/ASEE Joint Propulsion Conference and Exhibit, Cincinnati, OH, July 8-11, 2007

[4]. V. N. Smelyanskiy, V.V. Osipov, D. G. Luchinsky, D. A. Timucin, IEEE JANNAF Aerospace 2007, Denver, Colorado, 2007

[5]. V.V. Osipov, D.G. Luchinsky, V.N. Smelyanskiy, S-H Lee, C. Kiris, and D.A. Timucin, Aerospace Conference, 2007 IEEE, 3-10 March, BigSky, Montana, 2007 Page(s):1 – 16

[6]. D.G. Luchinsky, V.V. Osipov, V.N. Smelyanskiy, D.A. Timucin, Dogan, S. Uckun, Aerospace Conference, 2008 IEEE, 1-8 March, BigSky, Montana, 2008 Page(s):1 – 15

[7]. M.Salita, AIAA-2001-3443, AIAA/ASME/SAE/ ASEE Joint Propulsion Conference and Exhibit, 37th, Salt Lake City, UT, July 8-11, 200

[8]. P. Hill and C. Peterson, Mechanics and Thermodynamics of Propulsion, 2-rd ed., Addison-Wesley Publishing Company, Inc. New York, 1992.

[9]. D.R. Bartz, Heat Transfer from Rapidly Accelerating Flow of Rocket Combustion Cases and from Heated Air, in Advances in Heat Transfer, vol. 2, Hartnett, J. P. , and Irvine, T. F. Jr., eds., New York: Academic Press, 1965.

[10]. Handbook of Heat Transfer Application, 2-rd ed, Rohsenow, W. M. , Hartnett, J. P. and Ganic, E. N. , eds., McGraw-Hill Book Company, New York, 1973.

[11]. A. Peretz, K.K. Kuo, L. Caveny, and M. Summerfield, "Starting Transient of Solid Propellant Rocket Motors with High Internal Gas Velocities", AIAAJ Vol.11 No.12,12/73, pp 1719-27

[12]. Knoll DA, Chacon L, Margolin LG, Mousseau VA. "On balanced approximations for time integration of multiple time scale systems", J. Comput. Phys. 2003;185(2):583-611

BIOGRAPHY

Dr. **Dmitry G. Luchinsky** is a senior research scientist in MCT Inc. He obtained his MSc and PhD in physics in Moscow working on nonlinear optics of semiconductors. He is an author of more than 100 publications. He has been on a number of occasions a Royal Society Visiting Fellow and a NASA visiting scientist. He worked as a senior scientific researcher in VNII for Metrological Service (Moscow, Russia) and as a Senior Research Fellow in Lancaster University (Lancaster, UK). His research interests include nonlinear optics, stochastic and chaotic nonlinear dynamics, dynamical inference, fluid dynamics, ionic motion. His research is currently focused on theory and CFD of gas dynamics and fluid structure interaction in SRBs.

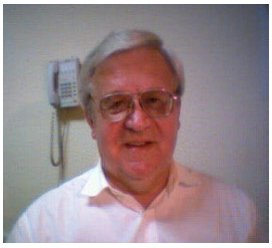

Dr. **Viatcheslav (Slava) V. Osipov** is a leading research scientist in MCT working at NASA Research Centre on nonlinear spatial extended systems far from equilibrium with application to semiconductor physics and hydrodynamics. Slava Osipov received MS, Engineer-Physicist followed by Ph.D. and Sci. Doc. in Physics of non-equilibrium systems" (1975) from Moscow Institute of Physics and Technology (MIPT) for the study of self-organization phenomena in physical, chemical, and biological system. He was a professor in MIPT and a science-director of the Department of Fundamental Research and Theoretical Physics in Russian State Science Center "ORION", Moscow, Russia. Dr. Osipov has published 4 books and more than 250 science articles in the leading physical journals. He have worked a research professor in scientific laboratories of different countries, including in Consejo Superior de Investigaciones Cientificas, Madrid, Spain, in University of New South Wales (UNSW), Sydney, Australia, and in Hewlett-Packard Labs, CA, USA.

Dr. **Vadim N Smelyanskiy** leads the physics modeling group in Computation Science Division at NASA Ames Research Center. He has obtained his BS, MS, and PhD in Institute of Semiconductors (Kiev, Ukraine). He has worked as a consultant and research Scientist in Los Alamos National Lab., Departments of Physics in Ann Arbor, MSU, and Princeton. Currently his research interest include nonlinear dynamics, statistical mechanics, Bayesian Statistics, nonlinear modeling, computer vision, quantum, computer, fluid dynamics of solid rocket motors, nonlinear dynamics of CMG.

Dr. **Dogan Timucin** leads the Modeling, Learning, and Control Group at NASA Ames Research Center. He holds BS, MS, and PhD degrees in electrical engineering, and has conducted research in the areas of optical and quantum computing, holographic data storage, and optical remote sensing. He is currently focused on the application of Bayesian state estimation and model reconstruction techniques to such problems as solid rocket motor failure detection and diagnosis, aircraft wiring integrity monitoring, and air traffic flow management.